

Optimal Maneuver-based Navigation for Cruising AUVs

by

KIM Kangsoo*

Abstract

We propose optimal maneuver-based navigation for a cruising AUV during near-bottom flight. To ensure vehicle safety as well as high-definition bottom survey, we optimize the reference depths of our waypoints using gradient-based numerical schemes. To increase the speed of convergence and numerical robustness, the numerical scheme is strengthened by the Broyden-Fletcher-Goldfarb-Shanno algorithm. By following the waypoints of optimized reference depths, an underactuated cruising AUV can carry out the waypoint-based optimal maneuver flight while avoiding a bottom collision. While the objective of our optimization is to minimize the difference between the reference and result trajectory, the reference depths assigned to waypoints are used as control inputs. In our optimization, along-track bottom bathymetry is incorporated as a constraint, and a dynamic model of a specific AUV is included as another constraint. Motion responses of the vehicle following the reference waypoints are derived by solving the dynamic model in the time domain. Our proposed approach has been validated by the simulations applied to a bathymetry model of actual undersea sites.

* Offshore Advanced Technology Department

Received January 26th, 2022.

Accepted February 28th, 2022

Contents

1. Introduction	77
2. Longitudinal Motion Control	77
2.1 Longitudinal Vehicle Dynamics	78
2.2 Depth and Altitude Control	78
3. Navigation	79
3.1 Waypoint Navigation	79
3.1.1 Bottom-following Navigation	79
3.1.2 Navigation by Optimal Maneuver	80
4. Numerical Solution Procedure	81
5. Simulations	83
5.1 AUV NMRI C-AUV #4	83
5.2 Vehicle Dynamics	83
5.3 Simulation Results	83
5.3.1 Results by Gradient Descent Search	84
5.3.2 Results by BFGS	85
6. Conclusions	86
Acknowledgment	87
References	87

Nomenclature

d_i, d_r	: current, reference vehicle depth [m]
e_d, e_h	: depth, altitude error [m]
e_θ	: pitch error [deg]
\mathbf{G}	: gradient vector of performance index [m]
\mathbf{H}	: Hessian matrix of performance index
h	: vehicle altitude at an arbitrary position [m]
h_i, h_r, h_a	: current, reference, minimum allowable vehicle altitude [m]
J	: performance index in optimal maneuver [m ²]
K_{pd}, K_{id}, K_{dd}	: proportional, integral, differential gain for depth controller
$K_{p\theta}, K_{i\theta}, K_{d\theta}$: proportional, integral, differential gain for pitch controller
q	: pitch rate [deg/s]
\mathbf{V}	: velocity vector [m/s]
w	: heave velocity [m/s]
x_0, x_l	: lower and upper limit of the along-track coordinate within a track [m]
z_t, z_v	: z-coordinates of target and vehicle trajectory [m]
α	: stepsize
γ	: flight-path angle [deg]
δ_e	: elevator input [deg]
ε	: tolerance parameters for stopping criteria
κ	: learning-rate parameter
ζ	: control vector [m]

1. Introduction

The recent advancement of submersible technology has enabled the epoch-making sea bottom survey of high resolution. Providing far higher resolution bottom survey data than is obtained from surface vessels, AUVs are increasingly being used in a range of ocean development applications in diverse sectors¹⁾. In the missions for diverse purposes, an AUV is often required to follow a bottom maintaining a fixed altitude above it. This navigation is called bottom following, considered as one of the primary strategies for near-bottom survey^{2,3)}. It is needless to say that the closer an AUV gets to the bottom, the higher the resolution of its survey data. At the same time, however, as its altitude from the bottom decreases, an AUV is faced with a higher risk of bottom collision. That is, while a low-altitude bottom following is highly useful for achieving high-resolution bottom survey, it takes higher risk of bottom collision. It is easily imagined that the risk of bottom collision gets more serious as the bottom provides rugged and steep terrain.

In general, AUVs are classified into two categories according to their behavioral character: hovering and cruising⁴⁾. The most outstanding difference between cruising AUVs and hovering ones is the underactuated character in vehicle dynamics. While a hovering AUV can hover and maneuver around an operating point, most cruising AUVs cannot^{5,6)}. This is because most cruising AUVs are underactuated, which means have restricted controllability⁵⁾. Due to this restriction in vehicle motion, a cruising AUV has difficulty in avoiding impending collision with the obstacles in close proximity, which discourages it from flying over a steep and rugged terrain.

As a sensor for detecting sea bottom, most AUVs use an active sonar. Single or multi beam echo sounder, ADCP (Acoustic Doppler Current Profiler), and profiling sonars are examples of sonars used for such purpose. These sonars are often called bottom-lock sonars, since they emit acoustic rays downwards, locking on a sea bottom. The situation that a bottom-lock sonar fails in detecting a sea bottom is called loss of bottom lock. Once there happens a loss of bottom lock, an AUV loses its current altitude above the bottom⁶⁾. This is such a dangerous state for vehicle safety, since any collision avoidance maneuver cannot be invoked without accurate information of the distance to surrounding obstacles. In the literatures^{7,8)}, it is proved that the loss of bottom lock is particularly liable to occur when a cruising AUV is flying over a steep and rugged terrain. This feature, together with the underactuated nature of vehicle dynamics makes near-bottom flight of a cruising AUV over a steep and rugged terrain difficult, posing far more significant risk of bottom collision.

In this research, we present an optimal maneuver-based navigation for the near-bottom flight of a cruising AUV. The optimal maneuver is achieved by following optimal waypoints. The optimal waypoints are the waypoints whose reference depths have been optimized. It is noted that collision avoidance strategy is incorporated into the waypoint optimization in our approach. For this, an along-track bottom-following trajectory is used as the target trajectory in optimizing reference depths of waypoints.

It is well known that any practical solution procedure of an optimization problem relies on an iterative numerical scheme. Therefore, when considering onboard implementation of an optimization problem, computation time matters significantly. In optimizing our waypoints, gradient-based numerical schemes are applied. Towards the onboard implementation of our approach, we present an advanced numerical scheme based on Broyden-Fletcher-Goldfarb-Shanno (BFGS) algorithm^{9,10)}. By adopting BFGS algorithm, we have achieved higher robustness, as well as faster convergence. In this research, by comparing with the results obtained by conventional gradient-based scheme, we show the efficacy of BFGS scheme in our problem.

2. Longitudinal Motion Control

The longitudinal control of a cruising AUV is a motion control exercised for adjusting its motion in vertical plane. In most cases, it is the depth below the surface or the altitude above the bottom that is used as the controlled variable for the longitudinal motion control of an AUV²⁾. For a near-bottom flight, in particular, bottom-following navigation is a prevailing approach applied to many cases of field applications^{3,4)}.

2.1 Longitudinal Vehicle Dynamics

In order for a cruising AUV to change its position within a vertical plane, it has to change its attitude beforehand. To take advantage of the lift force as well as reduce the drag force acting on the fuselage, a cruising AUV gets the nose-up (positive flight-path angle) during ascent and the nose-down (negative flight-path angle) during descent, as depicted in Fig. 1.

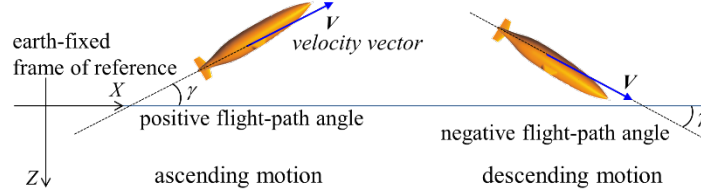


Fig .1 Typical longitudinal motions of a cruising AUV: ascent and descent.

2.2 Depth and Altitude Control

In the absence of significant disturbance, depth control of a submersible is simple and straightforward. Using current vehicle depth of great accuracy and reliability offered by a pressure sensor, depth control can be achieved successfully by using a finely-tuned feedback controller⁷.

Altitude control works on the basis of the altitude error defined as the difference between the reference and the current altitude of a vehicle. It is noted that, however, by substituting the altitude error with its depth error counterpart, a depth controller is also able to exercise the altitude control equivalently. Therefore, it is quite common that a depth controller of an AUV is also in charge of the altitude control^{4,8}. From Fig.1, we can easily understand that if the bottom bathymetry holds

$$e_d = d_r - d_i = h_i - h_r = -e_h \tag{2.1}$$

where e_d is the depth error and e_h is the altitude error counterpart of e_d . And, d_i and d_r are current and desired (reference) vehicle depths, while h_i and h_r are their altitude counterparts, respectively.

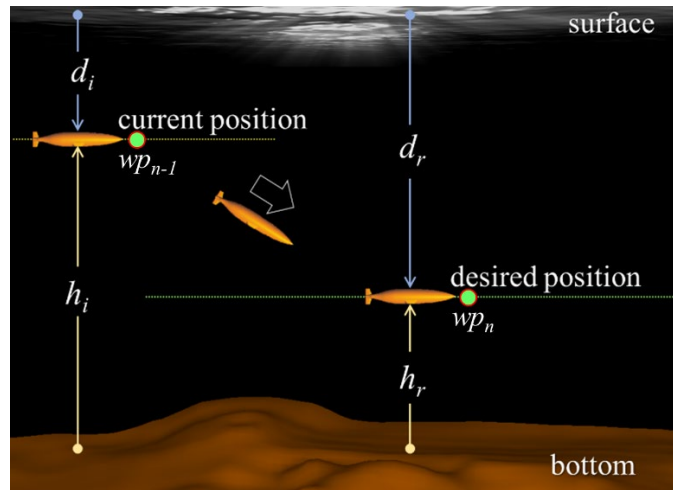


Fig. 2 Depth or altitude control of a cruising AUV.

Once e_d or e_h has been evaluated, it is fed to a feedback control architecture, such as PID (Proportional-Integral-Derivative) or lead-lag compensator. Figure 3 shows the schematic of the depth (altitude) control implemented employed in this research. As seen in the figure, our depth control is composed of twofold feedback loops. While depth is controlled in the outer loop, by referring to the pitch reference proportional to e_d , the pitch to elevator control is nested inside. Therefore, in the process of our depth control, the pitch control is always running implicitly.

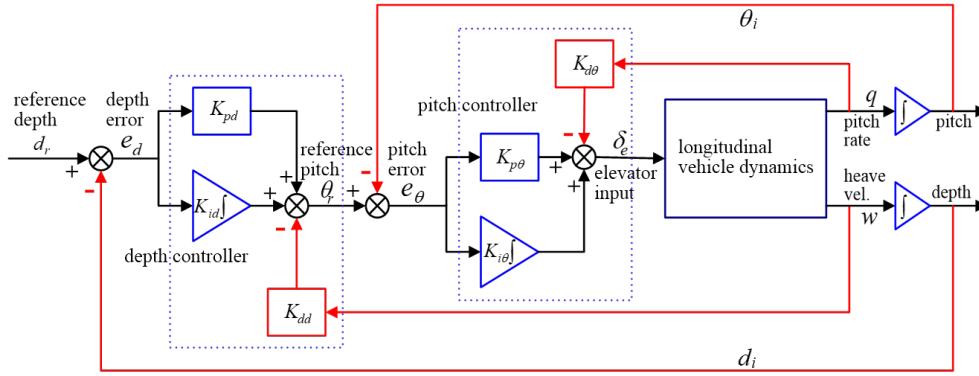


Fig. 3 Depth control schematic of a cruising AUV.

3. Navigation

3.1 Waypoint Navigation

Most of AUVs currently working in the world are operated on the basis of waypoint navigation. A waypoint is a set of 3D coordinates identifying the navigational points defined as the latitude, longitude, and depth or altitude pairs. Within the framework of waypoint navigation, a vehicle moves toward a destination passing through the reference waypoints. In our waypoint-based AUV navigation, the reference depth d_r of n -th waypoint (i.e., wp_n shown in Fig. 1) is the desired depth to be reached by a vehicle during its transit between wp_{n-1} and wp_n . Therefore, no sooner has the vehicle arrived at wp_{n-1} , its target vertical position is updated to the reference depth of wp_n .

3.1.1 Bottom-following Navigation

As mentioned previously, bottom-following navigation is preferably applied to a near-bottom flight of an AUV. In implementing bottom-following navigation, the availability of continuous vehicle altitude of accuracy is indispensable. In our previous work, however, we showed that the bottom-following navigation over a steep and rugged terrain can be the easiest trigger to bring about loss of bottom lock⁸⁾. Once happens, loss of bottom lock makes any bottom-lock sonar observation unavailable. Figure 4 shows typical behaviors of the vehicle pitch and altitude when a loss of bottom lock occurs. As noticed, losing the information of current true altitude, an underwater vehicle experiences drastic fluctuation in its pitching motion.

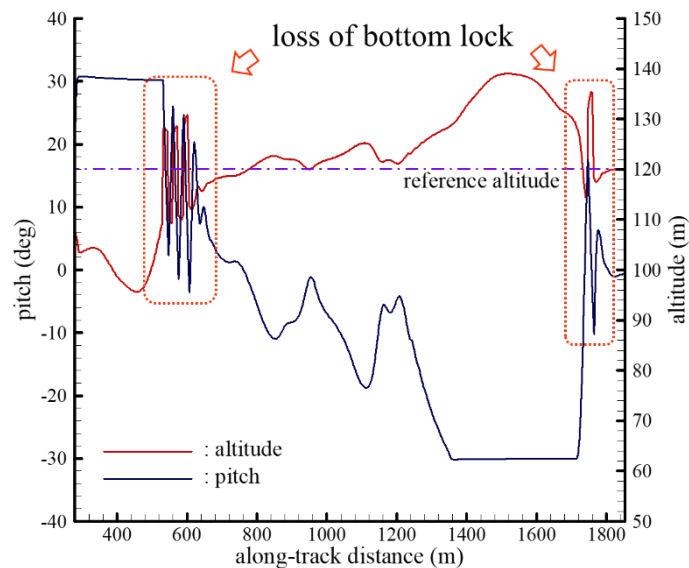


Fig. 4 Pitch and altitude of a cruising AUV experiencing loss of bottom lock.

Loss of bottom lock occurs when the received signal-to-noise ratio (SNR) decreases below a machine-specific threshold value. It is well known that the acoustic intensity of a scattered sound on the bottom, i.e., the bottom strength (BS), is strongly dependent on the incidence angle of an impinging acoustic ray^{8,11}). Having its maximum value at zero incidence angle, BS decreases rapidly as the incidence angle increases. Therefore, it is easily presumed that over a steep and rugged terrain, a bottom-lock sonar in operation is susceptible to loss of bottom lock. For the details of the generation mechanism of loss of bottom lock, refer to 8) and 11).

It is noted that in Fig. 4, the altitude shown is not the true but the indicated altitude, including large measurement errors due to drastic pitch fluctuation. This means a loss of bottom lock makes a vehicle blind to its true altitude, posing a risk of bottom collision. If the bottom above which an AUV is flying is steep and rugged, the vehicle is exposed to far greater risk of bottom collision. As seen above, we notice that bottom-following navigation may lose its adequacy in case being applied to an underactuated AUV subjected to a near-bottom survey over a steep and rugged bottom.

3.1.2 Navigation by Optimal Maneuver

As an alternative for the bottom-following navigation, we propose an optimal maneuver-based approach for the near-bottom flight of a cruising AUV. Within the category of the waypoint navigation, our approach optimizes the reference depths of waypoints. The optimal maneuver is accomplished by following the optimal waypoints. The set-up of the problem includes the waypoints predefined in horizontal plane with their sequence, i.e., the tracklines, along-track bottom bathymetry, and dynamic model of a specific AUV. Figure 5 depicts the basic concept of our approach. The waypoint optimization is performed in a track-wise manner. Within the track between $[wp_{n-1}, wp_n]$, for example, the reference depth of terminal waypoint is wp_n is optimized so as to make the result trajectory as close to the target trajectory, as possible. The target trajectory is an envelope of the along-track bottom section shifted upward by the reference altitude h_r . The value of h_r is arbitrary but should be set to be larger or equal to h_a , the minimum allowable altitude, introduced for exercising collision avoidance to the bottom.

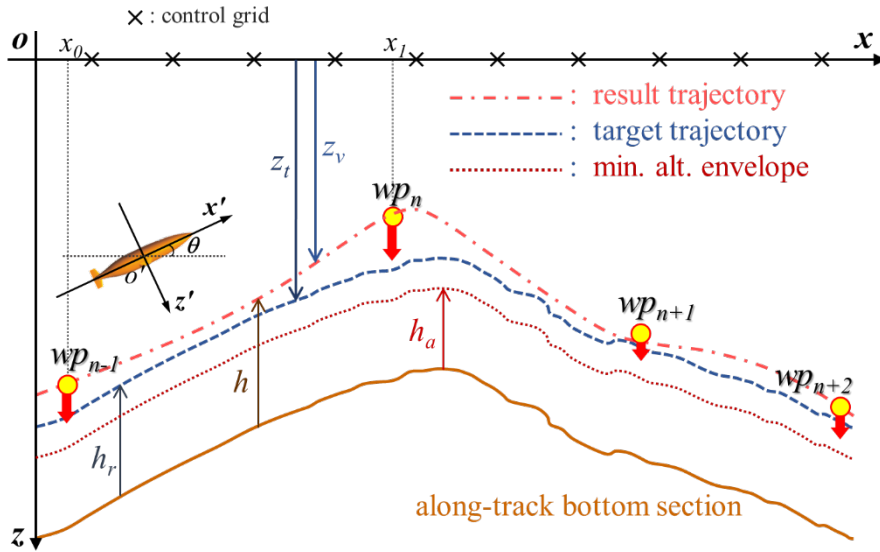


Fig. 5 Optimal maneuver-based navigation by waypoint optimization.

The problem of abovementioned optimal maneuver-based navigation is formulated as follows. As already mentioned, the objective of our optimal navigation problem is to derive the waypoint set that minimizes the deviation between the given target trajectory and the result trajectory obtained as a flight path. Therefore, the performance index of the problem is

$$J = \frac{1}{2} \int_{x_0}^{x_l} \|z_t(x) - z_v(x)\|^2 dx \quad (3.1)$$

where z_t and z_v are z -coordinates of the target and result trajectory, respectively. From the definition of the minimum allowable altitude, along-track vehicle altitude $h(x)$ should satisfy following condition.

$$h(x) \geq h_a \quad \text{for} \quad x \in [x_0, x_f] \quad (3.2)$$

Using Taylor series, we can expand J about the current point on the error surface of the control vector. From the definition of our problem explained above, we notice that the control vector is the z -coordinate of wp_n , denoted by z_{wp1} . Therefore, the Taylor series takes the form as

$$J[z_{wp1} + \Delta z_{wp1}] = J[z_{wp1}] + \mathbf{G}^T \Delta z_{wp1} + \frac{1}{2} \Delta z_{wp1} \mathbf{H}(n) \Delta z_{wp1} + O(\varepsilon^3) \quad (3.3)$$

where $O(\varepsilon^3)$ denotes third or higher order terms. In (3.3), \mathbf{G} is the gradient vector defined by

$$\mathbf{G} = \left. \frac{\partial J}{\partial z_v} \right|_{z_v = z_{wp1}} \quad (3.4)$$

Also, \mathbf{H} is the local Hessian matrix defined by

$$\mathbf{H} = \left. \frac{\partial^2 J}{\partial z_v^2} \right|_{z = z_{wp1}} \quad (3.5)$$

In the method of Cauchy's gradient descent search, exemplified by the back-propagation algorithm, the update amount of control vector is defined by

$$\Delta z_{wp1} = -\kappa \mathbf{G} \quad (3.6)$$

where κ is so called the learning-rate parameter¹²⁾.

4. Numerical Solution Procedure

Numerical solution of the control vector is derived by a numerical solution procedure working in an iterative manner. In our solution procedure, the control vector z_{wp1} is updated at every iteration step by using the update amount (3.5). In evaluating Δz_{wp1} , we must determine a well-suited value of κ . In many cases, an appropriately selected constant value of κ is used. The learning rate κ , however, exerts a dominant influence on the accuracy and stability of the solution, as well as the convergence. Improper selection of κ may bring about the divergence at worst, or the unacceptable accuracy and slow convergence, even if a failure in numerical calculation is avoided. Taking notice of this, we employ an advanced search algorithm called BFGS^{10,11)}, in deriving the numerical solution of our problem. BFGS is a gradient-based technique, belonging to the family of Variable Metric Methods (VMM). By carrying forward information from the previous iterations, BFGS assures the property of quadratic convergence. By applying BFGS algorithm, the optimal control vector is derived as follows.

At first, we choose a positive definite initial metric \mathbf{A} . Also, we select appropriate values of ε_1 and ε_2 , the tolerances for stopping criteria. In BFGS, the search direction is obtained as a solution to

$$\mathbf{A}_i \mathbf{s}_i = -\mathbf{G}_i(\boldsymbol{\zeta}_i) \quad (3.7)$$

where i denotes current iteration step. In (3.7), $\boldsymbol{\zeta}_i$ represents the control vector at i -th iteration step, that is, z_{wpl} in our problem. In deriving \mathbf{s}_i , we perform a line search to obtain an acceptable stepsize α_i in \mathbf{s}_i direction. If the line search is completed properly, α_i satisfies

$$\alpha_i = \arg \min \{ \mathbf{G}(\boldsymbol{\zeta}_i + \alpha_i \mathbf{s}_i) \} \quad (3.8)$$

Then, the control vector is updated as

$$\boldsymbol{\zeta}_{i+1} = \boldsymbol{\zeta}_i + \alpha_i \mathbf{s}_i = \boldsymbol{\zeta}_i + \Delta \boldsymbol{\zeta} \quad (3.9)$$

Defining \mathbf{Y} such that

$$\mathbf{Y} = \mathbf{G}(\boldsymbol{\zeta}_{i+1}) - \mathbf{G}(\boldsymbol{\zeta}_i) \quad (3.10)$$

And next, we evaluate \mathbf{B} and \mathbf{C} as

$$\mathbf{B} = \frac{\mathbf{Y}\mathbf{Y}^T}{\mathbf{Y}^T \Delta \boldsymbol{\zeta}} \quad (3.11)$$

$$\mathbf{C} = \frac{\mathbf{G}(\boldsymbol{\zeta}_i)\mathbf{G}^T(\boldsymbol{\zeta}_i)}{\mathbf{G}^T(\boldsymbol{\zeta}_i)\mathbf{s}_i} \quad (3.12)$$

Using (3.10) and (3.11), \mathbf{A}_i is updated as

$$\mathbf{A}_{i+1} = \mathbf{A}_i + \mathbf{B} + \mathbf{C} \quad (3.13)$$

By applying (3.13) into (3.7) and repeating the sequential procedure of (3.8) ~ (3.13), we obtain the optimal value of $\boldsymbol{\zeta}$. In determining the convergence of $\boldsymbol{\zeta}$, we use one of the following stopping criteria.

$$\mathbf{G}^T(\boldsymbol{\zeta}_{i+1}) \mathbf{G}(\boldsymbol{\zeta}_{i+1}) \leq \varepsilon_1 \quad (3.14a)$$

$$|\mathbf{J}(\boldsymbol{\zeta}_{i+1}) - \mathbf{J}(\boldsymbol{\zeta}_i)| \leq \varepsilon_2 \quad (3.14b)$$

5. Simulations

We consider a realistic example that validates the efficacy of the optimal maneuver-based navigation. In this example, we use a bathymetry model of an actual undersea site, located in Northwestern Pacific, near Japan. The terrain of the site includes very steep slope, the maximum angle of which exceeds 40° .

5.1 AUV NMRI C-AUV #4

The AUV considered in this research is a cruising AUV developed and operated by National Maritime Research Institute (NMRI), Japan. Lunched in 2018, NMRI C-AUV #4 has accomplished several undersea missions of practical purposes. Figure 6 shows overall layout of C-AUV #4.

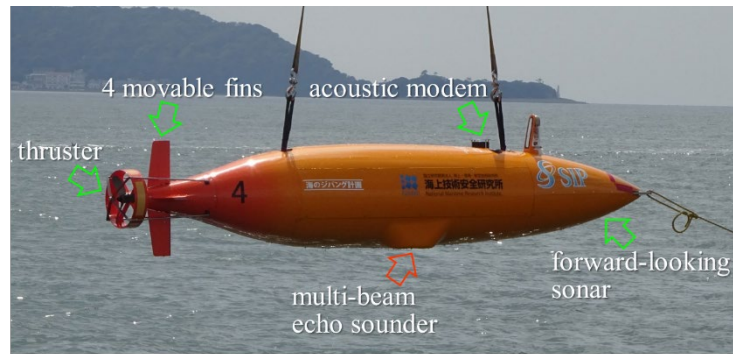


Fig. 6 Overall layout of NMRI C-AUV #4.

5.2 Vehicle Dynamics

In this simulation, the vehicle is assumed to translate uniformly with its cruising speed of U_0 . And in describing its longitudinal motion, a pitch dynamics model of the vehicle (3.15) is employed. (3.15) is a pitch to elevator deflection transfer function, derived by a system identification approach. In (3.15), q is the pitch rate of the vehicle in deg/s, while δ_e the elevator deflection in degree.

$$\frac{q}{\delta_e} = \frac{-0.173s}{s^3 + 2.681s^2 + 0.546s + 0.048} \quad (3.15)$$

5.3 Simulation Results

Figure 7 shows the waypoints within horizontal plane with their track interval superimposed on the bathymetric map of the site. As seen, six waypoints are to be optimized in order to accomplish an optimal maneuver-based flight along the trackline. Horizontal distribution of waypoints is arbitrary, determined considering the places to be visited for a given mission. In this example, the trackline covers highly steep ascending terrain, directing southward.

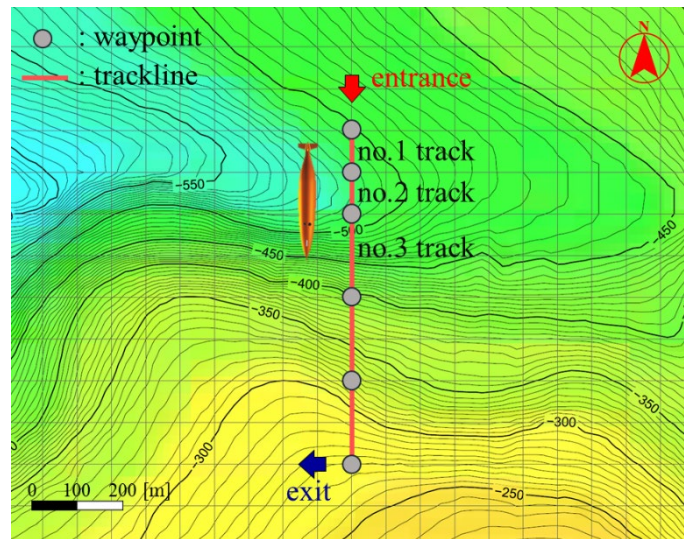


Fig. 7 Top view of the trackline and waypoints prepared for simulations.

5.3.1 Results by Gradient Descent Search

In the first case, conventional gradient descent search scheme in solving our optimal navigation problem. With a constant learning rate parameter, we set the maximum iteration to be 200. It is noted here that in this simulation, the reference altitude is set to be 80 m, while the minimum allowable altitude 60 m. Therefore, the along-track bottom section shifted upward by 80 m becomes the reference altitude envelope. Figure 8 shows the results of AUV flight following the optimal waypoints.

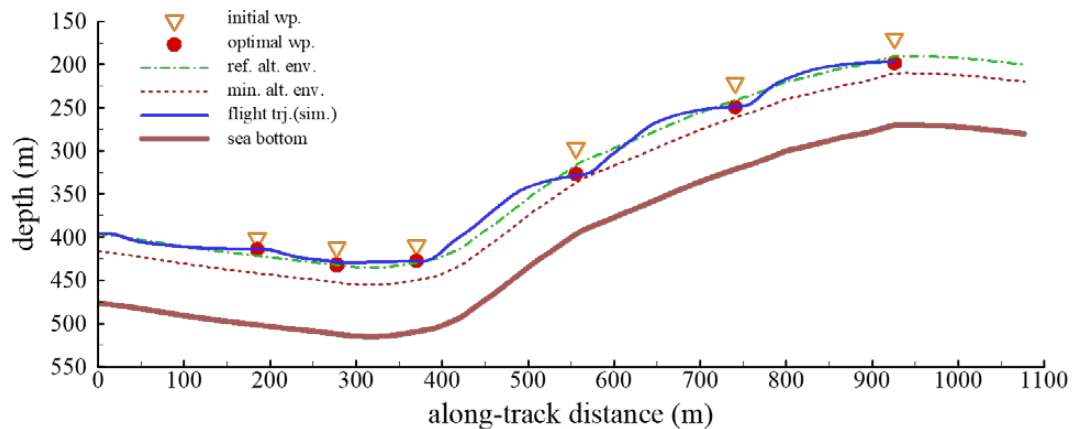


Fig. 8 Simulated AUV flight following optimal waypoints: result by conventional gradient descent search.

Following the optimal waypoints, C-AUV #4 flies over the bottom with the minimized deviation from reference altitude envelope. In Fig.8, blue solid line represents the vehicle flight trajectory following optimal waypoints. On the other hand, red dotted line represents the minimum allowable altitude envelope, while green dot-dashed line represents that of the reference altitude. It is noted that while the vehicle follows the optimal waypoints successfully, its flight trajectory remains above the minimum allowable altitude envelope. This means that avoiding bottom collision is successfully achieved by our optimal maneuver-based navigation.

The performance indices of first 3 tracks in the trackline is shown in Fig. 9. As seen in the figure, performance indices decrease monotonically, which means our gradient descent search schemes works properly. It is noted that while 200 iterations are required in no.3 track, converged solutions are obtained at smaller iterations in no.1 and no.2 tracks.

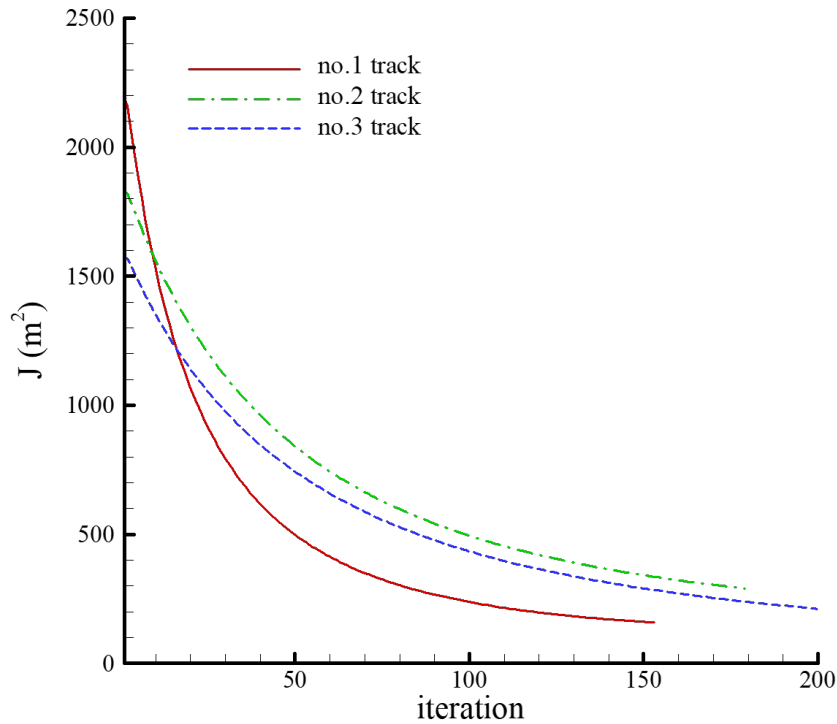


Fig. 9 Track-wise performance indices: results by conventional gradient descent search.

5.3.2 Results by BFGS

In the next case, we applied BFGS algorithm in deriving the optimal control vector. As was the case in gradient descent search, we set the maximum iteration to be 200. The reference altitude and the minimum allowable altitude are set to be the same values those used in previous example, which are 80m and 60 m, respectively. Figure 10 shows the AUV flight trajectory obtained by following the optimal waypoints.

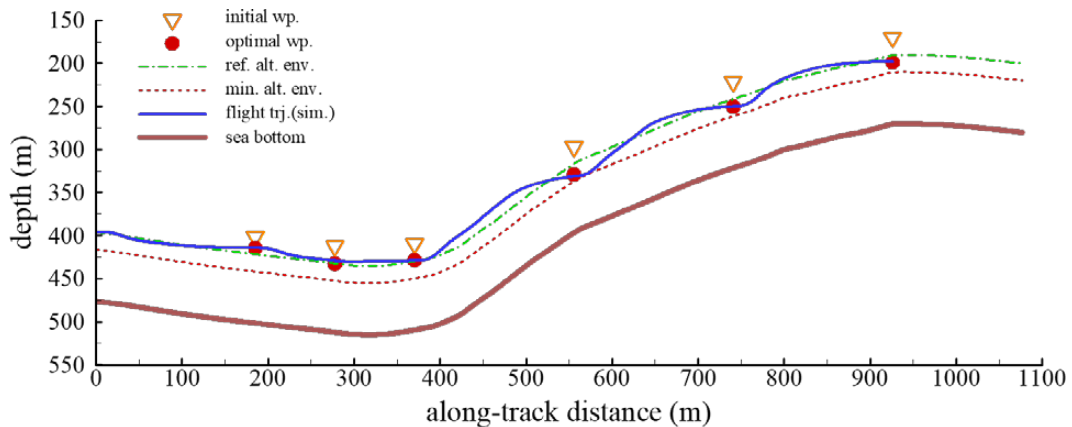


Fig. 10 Simulated AUV flight following optimal waypoints: result by BFGS.

By comparing Fig. 8 and Fig. 10, we notice that in essence, the flight trajectory obtained by BFGS shows no difference between the one by conventional gradient descent search. This means both algorithms have worked in a highly analogous manner, as well as effectively, leading to optimal control vectors in the vicinity of minima, even though it may not be the global one.

The track-wise performance indices with respect to iterations are given in Fig. 11. While there is no substantial difference between two flight trajectories, performance indices show obvious differences. As noticeable in Figs. 9 and 11, the final values of performance indices obtained by BFGS are more or less smaller than those obtained by conventional gradient descent search.

This implies BFGS leads to the optimal solutions of better convergences, although it hardly has practical meaning. In view of the computational effort, however, BFGS exhibits clear superiority. While the conventional gradient descent search requires at least 150 iterations in reaching the convergence, the maximum iteration number in BFGS is below 30. This is a great advantage, especially when considering an onboard implementation in which only a strictly limited computational power is available, in general. It needs to be noted here that the numbers of iterations required, as well as the final values of track-wise performance indices are strongly influenced by the along-track terrain profile of each track.

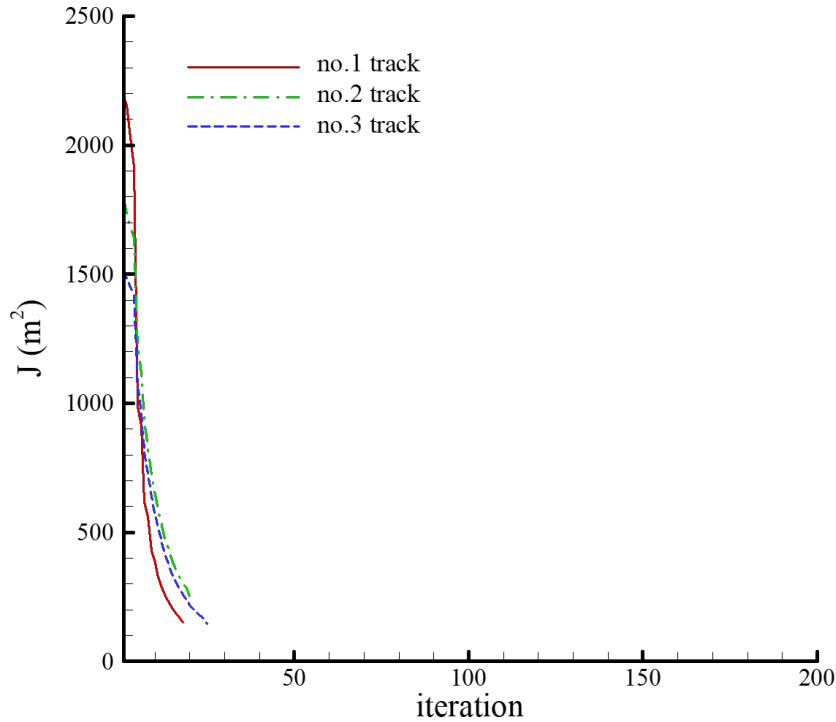


Fig. 11 Track-wise performance indices: results by BFGS.

6. Conclusions

A systematic approach for achieving optimal maneuver-based navigation has been developed and validated through simulations. Simulation results have shown that our optimal maneuver lets the vehicle follow the bottom in an approximate manner, minimizing the deviation between the reference and the optimized flight trajectory. This enables a quasi bottom-following flight of a cruising AUV, keeping on exploiting the advantages of depth-based navigation, such as the measured control output of high reliability.

Based on waypoint-based depth control, our approach can easily be implemented on most of AUV systems in operation. In deriving optimal waypoints, we assessed two gradient-based numerical schemes: the conventional gradient descent search and the BFGS. Though there is not substantial difference between the converged solutions by two approaches, BFGS has exhibited faster convergence. Fast and robust convergence is especially important for real-time onboard implementation. Thus, BFGS can be a viable candidate for future onboard implementation of our scheme. Through the simulations of AUV flight over a steep terrain located in an actual undersea site, we found that our optimal maneuver successfully prevents from bottom collision. Consequently, it can be said that our approach accomplishes depth-based optimal maneuver flight, avoiding bottom collision.

Acknowledgment

This work is partly supported by Council for Science, Technology and Innovation (CSTI), cross-ministerial Strategic Innovation Promotion Program (SIP), next-generation technology for ocean resources exploration (lead agency: JAMSTEC).

References

- 1) Wynn, B. et al.: Autonomous Underwater Vehicles (AUVs): Their past, present and future contributions to the advancement of marine geoscience, *Marine Geology*, Vol. 352(2014), pp. 451-468.
- 2) Caccia, M., Bruzzone, G., and Veruggio, G.: Bottom-following for remotely operated underwater vehicles: Algorithms and experiments, *Autonomous Robots*, Vol. 14(2003), pp. 17-32.
- 3) Yoerger, D.R., Jakuba, M., Bradley, A.M. and Bingham, B.: Techniques for deep sea near bottom survey using an autonomous underwater vehicle, *Int. J. of Robotics Research*, Vol. 26(2007), pp. 41-54.
- 4) McPhail, S., Furlong, M. and Pebody, M.: Low-altitude terrain following and collision avoidance in a flight-class autonomous underwater vehicle, *Journal of Engineering for the Maritime Environment*, Vol. 224, No. 4(2010), pp. 279-292.
- 5) Lea, R.K., Allen R. and Merry S.L.: A comparative study of control techniques for an underwater flight vehicle, *Int. J. of System Science*, Vol. 30, No.9(1999), pp. 947-964.
- 6) German, C.R. and Parson, L.M.: RRS "Charles Darwin" Cruise 169, Hydrothermal exploration of the southern Mid-Atlantic Ridge, National Oceanography Centre Southampton Cruise Report 6 (2006), Southampton, UK.
- 7) Kinsey, J.C. et. al: A survey of underwater vehicle navigation: recent advances and new challenges, *Proc. IFAC Conference of Manoeuvring and Control of Marine Craft*, Lisbon, Vol. 88(2006), pp. 1-12.
- 8) Kim, K. and Ura, T.: Navigation Strategies of a Cruising AUV for Near-bottom Survey of a Steep Terrain, *IFAC-PapersOnline*, Elsevier, Vol. 49, No. 15(2016), pp. 75-80.
- 9) Brayden, C. G.: The convergence of a Class of Double-rank Minimization Algorithms, *IMA Journal of Applied Mathematics*, Vol. 6, Issue 1(1970), pp. 76-90.
- 10) Fletcher, R.: A New Approach to Variable Metric Algorithms, *The Computer Journal*, Vol. 13, Issue 3(1970), pp. 317-322.
- 11) Urlick, R.J.: *Principles of Underwater Sound* (3rd edition), McGraw-Hill(1983), ISBN 0-07-066087-5.
- 12) Goh, A. T. C.: Back-propagation Neural Networks for Modeling Complex Systems, *Artificial Intelligence in Engineering*, Vol. 9, Issue 3(1995), pp. 143-151.